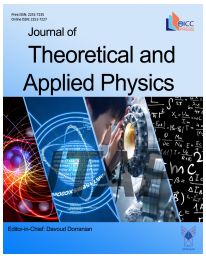

Volume 17, Issue 5, 172350 (1-14)

Journal of Theoretical and Applied Physics (JTAP)

https://dx.doi.org/10.57647/j.jtap.2023.1705.50

The effect of powered needle-electrode geometry on the RF plasma jet

Seyyed-Jalal Pestehe*, Davood Hassanpour

Advanced Plasma Laboratory, Faculty of Physics, University of Tabriz.

***Corresponding author**: sjpest@yahoo.com

Received 29 May 2023; Accepted 02 August 2023; Published Online 06 October 2023 ORIGINAL RESEARCH

Abstract:
An atmospheric pressure plasma microjet device with a tapered ground electrode and dielectric barrier is developed. The effects of the powered electrode geometry and input power on the specifications of the launched RF plasma jets are investigated. Needle-powered electrodes with different types, shapes, lengths, and diameters, such as perforated and un-perforated hollow cylindrical tubes with different inner and outer diameters or solid with flat tip and with sharp tip steel nail rods are examined. The effects of the discharge gap size on the launched jet lengths and widths are studied. The axial and radial components of the electric field are simulated at the device output nozzle by applying radiofrequency power to the needle electrode and their possible effects on the plasma plume generation are discussed. The variations of the launched microjet lengths and widths are investigated versus the working gas (argon) flow rates in two experiments with two different fixed input powers. It has been shown that there is an optimum flow rate to obtain maximum jet length with a suitable narrow width. The effects of nozzle diameter, how to inject gas into the system, and argon flow rates on the plasma plume characteristics are discussed through the Reynolds number.

Keywords: Atmospheric pressure plasma jet; Powered electrode geometry; Hollow electrode effect; Jet length; Laminar-to-turbulent transition

1. Introduction

Non-thermal plasmas have been utilized in different fields, such as surface treatment for cleaning, sterilization, protective coatings and analysis, environmental refinement, biological and medical treatments, at broad range of pressures [1–4]. These plasma sources, have to meet stringent requirements such as low temperature, no risk of arcing, operation at atmospheric pressure, preferably hand-held operation, and low concentration of ozone generation, therefore reliable and user-friendly of this kinds of sources need to be developed. The non-equilibrium plasmas impose a low temperature to the substrates during treatment, allowing the exposure of fragile surfaces such as polymers, papers, or biological thermo-sensitive cells.
Among other approaches, capillary plasma jets are capable of generating and stabilizing non-thermal plasmas at atmospheric pressure in a relatively wide range of geometries and dimensions. They can be miniaturized for a local treatment of non-flat, structured 3D surfaces such as cavities and trenches in the sub-millimetre range [5].

Several geometries have been proposed to generate non-thermal plasma jets using different power sources in a wide range of frequencies including radiofrequencies. It can be said that the first generation of uniform non-equilibrium radiofrequency atmospheric pressure plasma jet RF APPJ has been reported by Jeong and co-workers [6] using helium as the working gas, following the report of Koinuma and colleagues on micro beam plasma generator [7]. Jeong and colleagues have found the stable operation with helium flow rates of > 25 slm, together with 3.0%/4.0% of reactive gas, oxygen/carbon-tetrafluoride, concentration by volume, and RF power between 50 and 500 W. They have also found the helium to be essential to obtain a stable discharge. In addition, the happening of arc discharge, at the too high powers and too low gas flow rates, at the end of the centre electrode was reported. The uniformity of the glow between the electrodes was also investigated by the visual inspection of the discharge. They have mentioned, without referring to their measurement approach, that the gas temperature in their plasma jet could be as low as 100°C. Stoffels group [8] developed an RF plasma needle which could operate at

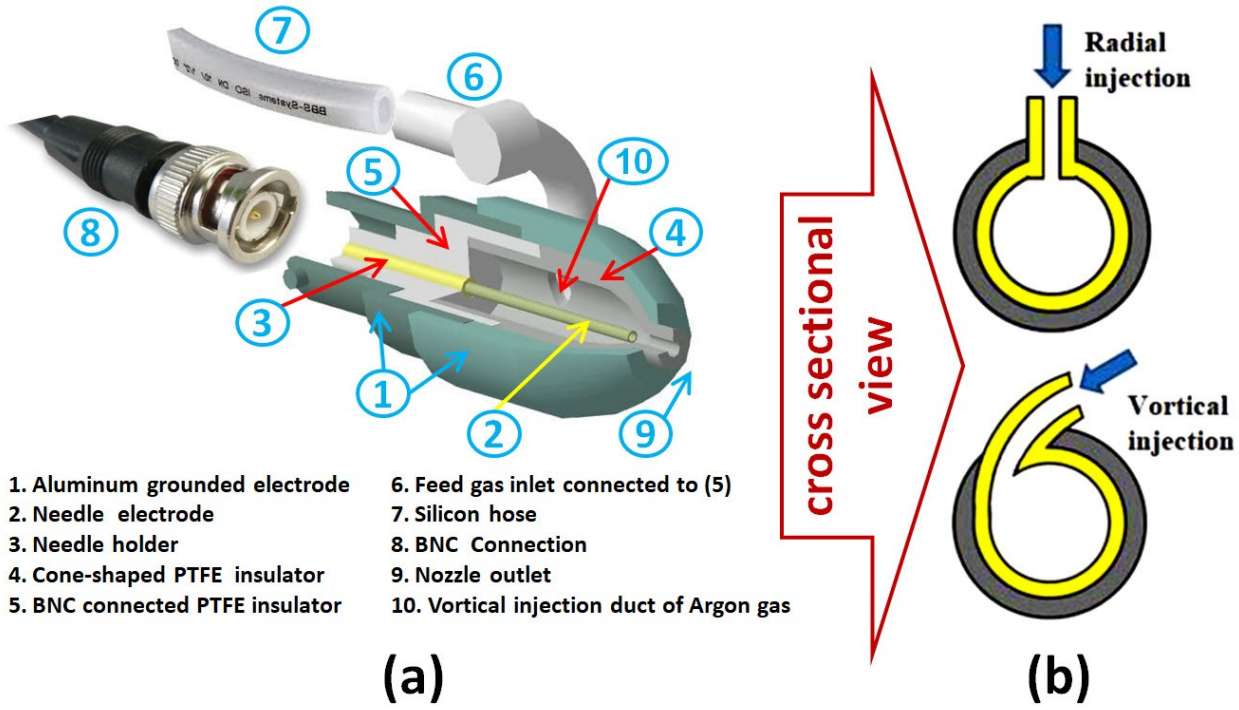

Figure 1. Schematic of the designed atmospheric pressure plasma microjet (APPμJ).

relatively low voltages ($200-500$ V peak-to-peak) with the power consumption of tens of milliwatts up to a few watts. They have also reported that excitation and vibration temperatures were close to each other ($0.2-0.3$ eV) and rotational gas temperature was at most a few hundred K. They found that at lowest power input the source had the highest excitation temperature while the gas remained at room temperature. They have, also, demonstrated that their device could be applied on organic materials, also in watery environment, without causing thermal/electric damage to the surface. Stonies and co-workers [9] developed a very small coaxial plasma source based on the microwave plasma torch which could generate a plasma jet up to 4 mm long at 2 W microwave power (2.45 GHz) at atmospheric pressure. The excitation temperature of the jet was found to be ~ 470 K when the device was operating with Helium and 17 W of microwave power. It was, also, thought to be a source for the atomic spectroscopy of gaseous species. In 2005, Teschke and colleagues [10] studied the propagation of kilohertz dielectric barrier APPJ and shown that the plasma jet device acts like a "plasma gun" blowing small "plasma bullets" out of its mouth. Laroussi and Lu [11] introduced a new structure to generate plasma jet using a pulsed DC (in the $1-10$ kHz range) source and reported a jet length of several centimetres. The plasma jet was sustained by a strong gas flow passing through the discharge region (in the $1-10$ slm range) and nearly low input power of 15 W. They reported that the length of the plume depends on the helium flow rate and the magnitude of the applied voltage pulses. They have also found that the plasma plume remained at low temperature and could be touched by bare hands without any harm.

Hong and Uhm [12] made use of Laroussi's jet structure with a hole diameter of about 500 μm and reported that by applying a 20 kHz high voltage to the powered electrode and letting N_2 flows from the back, a plasma jet up to 6.5 cm is generated in the surrounding air. They measured the gas temperature by a thermocouple and as showed that the temperature of the plasma jet at 2 cm from the dielectric case was below 300 K. They have reported that their micro plasma device could also produce a short plasma less than 5 mm in length such as the device known as the plasma needle [8]. Laan and colleagues [13] developed an RF driven plasma needle similar to Stoffels model [8] and generated a room temperature spherical glow with an average diameter of 1 mm. They proposed that a monitor of the dissipated discharge power can serve as a non-contact gap width (the distance between the needle tip and the surface) sensor, then, they developed this sensor and operated it for system diagnosing. In 2006, the van de Ven group developed a new DBD plasma needle to meet the criteria of reducing the working gas (helium) flow rate, device size and weight, having axial and modular structure [14]. This needle was specially designed to use a height sensor for their actuator. In 2006 Kim and co-workers [15] used a DBD pin to a dielectric plate structure driven by a $20-80$ kHz power supply and showed that the plasma characteristics could be controlled by geometrical and operational parameters of the experiment. In 2008, Kolb and colleagues built a millimeter-sized plasma microjet that operated with D.C. voltage. The outlet diameter of the nozzle was less than 1 mm and it created a plasma jet with a thickness of $1-2$ mm. They proposed the possibility of using a plasma microjet to treat heat-sensitive and small-size materials, e.g. plastics, or tissues such as skin [16]. In 2012 Zhu and Lope [17] generated a direct current, non-thermal, atmospheric-pressure plasma

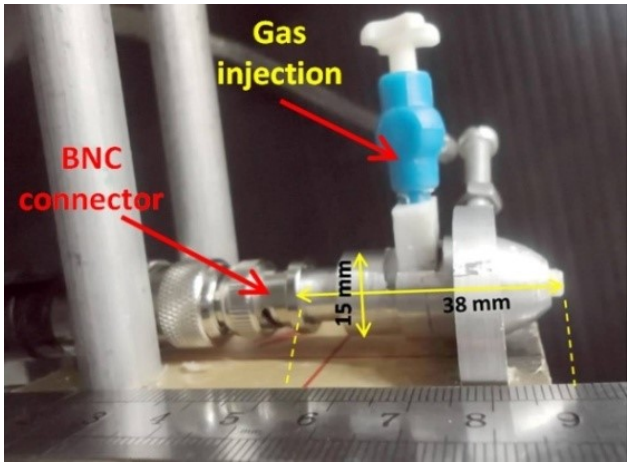

Figure 2. The constructed microjet.

microjet with helium/oxygen gas mixture as working gas, and investigated the jet length, electrical and optical properties, then, studied the generation and density of plasma species such as atomic oxygen, OH, Cu and ozone as a function of the oxygen concentration.

Sun and Wang and their co-workers in two separate works [18, 19] used plasma microjet in combination with other chemicals, in tooth-whitening. They compared the tooth-whitening effects of hydrogen peroxide enhanced by plasma microjet and the conventional clinical method of using H_2O_2 alone and reported a significant improvement of the tooth-whitening with the first one. In other work Pan et al. [20], studied the tooth-whitening effect of air plasma microjet in combination with 0.9% saline solution. They treated three groups of teeth for 20 min with an air blow and saline solution, a plasma microjet and saline solution, and 35% hydrogen peroxide gel. They reported that the teeth treated with the plasma microjet and saline solution showed the best tooth-whitening effect in comparison with the others. In another work Wang et al. [21], used Ar/O_2 (2%) microjet to disinfect root canals in single-rooted extracted human teeth and showed that 98.8%. Enterococcus faecalis was inactivated in 8 min. However, the seemingly cleaned root canal was reinfected after a week, possibly due to the hard-to-reach infected dentinal tubules. Bussiahn and co-workers [22] generated a hairline plasma with a length up to 1.5 cm to treat the tip of the root canal.

In the use of plasma microjet for surface cleaning, one can refer to Tajima et al. [23], as an example, in which an inductively coupled microjet was designed and used to treat CUO and Cu_2O films that are created readily on Cu surface specially at higher temperatures.

As one can easily deduces from the above discussion, the applications related to medicine, dentistry, and surface cleaning/treatments, specially tooth and antique surface bleaching, require microjets with small widths (< 1 mm) and long lengths (more that few millimetres) to access points located in depth, without damaging the surrounding media, which were not accessible otherwise. This kind of plasmas have to be cold (close to room temperature for processing temperature sensitive surfaces) with the ability of producing functional active species.

In this work, we have adopted a system similar to van de Ven group structure, keeping their criteria of reducing the gas flow rate, device size and weight, having axial and modular structure, to develop a tapered DBD-like plasma microjet with different structure of Teflon cap, grounded and powered electrode shapes and types. The effects of the powered electrode geometries, input RF powers and working gas flow rates on the length and width of the launched plasma jet are studied.

A DBD-like system is used in this work because by covering both of the electrodes, in the DBD structures, the electric field intensity associated with the applied potential decreases around the powered electrode, increasing the minimum power required for the jet ignition [24]. By covering only one of the electrodes by dielectric material, especially the grounded one, to obtain a DBD-like system, the electric field around the powered electrode can be high enough to lower the ignition power significantly.

2. Experimental setup and plasma jet aspects

Since we have developed our plasma jet inspired by the work of van de Ven group, we will explain it first. As mentioned in the previous section they developed their plasma needle to meet the criteria of reducing the working gas (helium) flow rate, device size and weight, and having axial and modular structure. They used a SMC-connector instead of using male BNC-connector, to put the radio-active tungsten wire (with 2% thorium) directly into the connector for miniaturisation purposes. The dimensions of the stainless steel cover (grounded electrode) was chosen so that the connector and the helium tube can be placed next to each other inside it and the coaxial cable and the helium inlet tube do not interfere. At the front of the needle, a Teflon cap with a central blind hole of 3 mm, in which the wire came through, was placed. To let the helium flow out of this hole nearly axially, 4 thirty degrees inclined holes of 1 mm diameter at right angle around the device axis were made in the Teflon cap. The connector and the Teflon cap are placed inside a stainless steel cover. In between the back of this cover and the cap, a helium chamber was placed

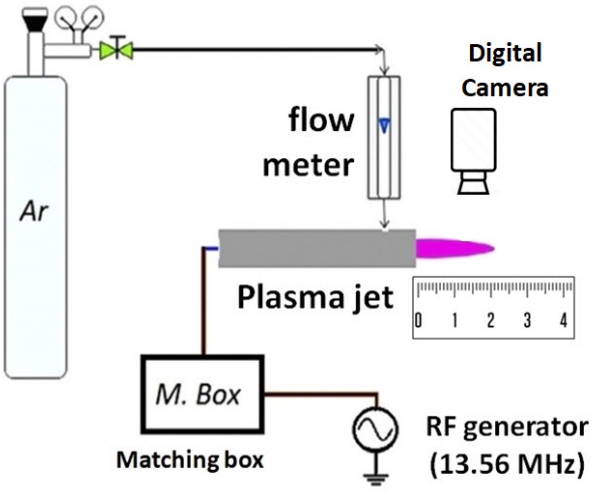

Figure 3. Schematic of experimental setup.

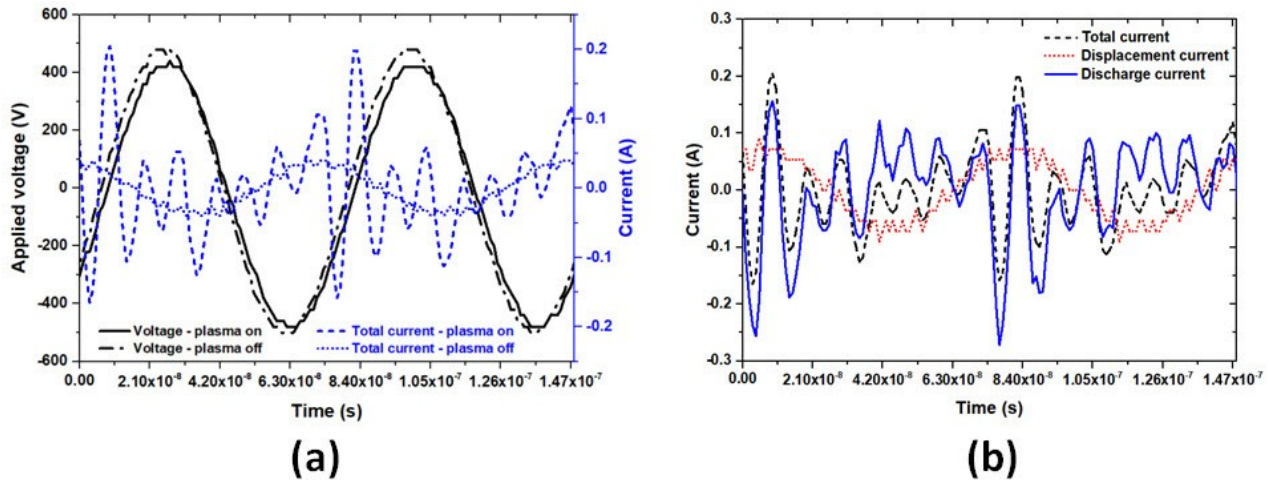

Figure 4. (a) The potential deference between the two powered and grounded electrodes as well as the experimentally measured current, with/without the plasma ignition, for 3 slm and 30 W applied power. (b) The experimentally measured currents in plasma on/off states as well as the resulted discharge current by subtracting them.

enabling the helium gas to scatter in the tangential direction before flowing through the 4 holes. The powered sharped-tip needle electrode was covered with a glass cover and the Teflon cap filled the space between the grounded and powered electrodes leading to a dielectric barrier discharge (DBD) structure. This needle was specially designed to act as a height sensor in examining the amount of reflected RF power during the device function as a sensor of the distance between the plasma and target. For this reason, the thickness of the Teflon cap has been considered non-uniform and high to reduce the radial electric field component in their device. Covering the needle electrode, also, would increase the input power requirement. It can be also said that the gas will not have enough time to get the laminar flow after leaving the inclined holes.

Choosing a tapered geometry for the outer grounded electrode, an atmospheric pressure plasma microjet (APPμJ) device is developed to overcome the above mentioned shortcomings and fabricated for further investigation on it. The system is designed such that the replacement of its parts to be very easy. The inner electrode, which could be a hollow cylindrical tube with different inner and outer diameters (here, medical syringes) or solid steel nail rod with the same diameter as the outer diameter of the used syringes, is powered using a built in BNC-connector and RG-213U coaxial cable via the RF L-type matching unit. The outer grounded electrode is shaved from aluminium in tapered shape so that the electrode thickness is 1 mm all over it. The isolating dielectric (here Polytetrafluoroethylene (PTFE)) between the two electrodes (Teflon cap) is shaved the same as the outer electrode and placed inside of it to cover its inner surface. With the same thickness of the Teflon cap, the amplitude of the radial electric field component will be sufficient to help for the fast bullet ejection from the nozzle [25]. This system may be put, globally, into DBD-like plasma jet category proposed by Lu et al. in 2012 [26]. The working gas entrance is designed so that the gas could be injected straight along the radial direction as well as with a vortex type motion with a possible maximum angular velocity as shown in Fig. 1b. The working gas in this study is chosen to be argon gas with 99.9% purity flowing with 3 slm flow rate generally.

Fig. 1a and Fig. 2 show the schematic and the image of the constructed APPμJ, respectively. As can be seen from Fig. 2, the length of the constructed prototype, measured from the BNC connection up to the output nozzle is 38 mm and its diameter is 15 mm, which can be made even smaller using sophisticated manners.

3. Inner electrode optimization

Several experiments were carried out by changing the type, shape, length, and diameter of the powered inner electrode. In all of these experiments, the inner electrode is powered by RF power generator (Basafan RFG03BF) with maximum

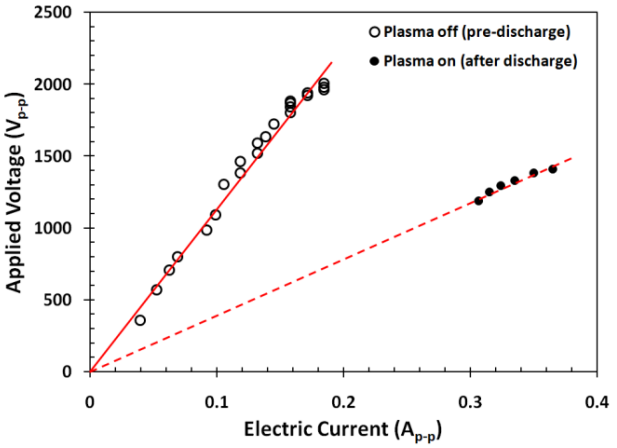

Figure 5. V – I characteristic curve for plasma on/off states. The peak-to-peak applied voltage was measured using a digital oscilloscope by averaging 256 samples through the H.V. Probe and the peak-to-peak jet current was measured using 3.3 nF capacitor.

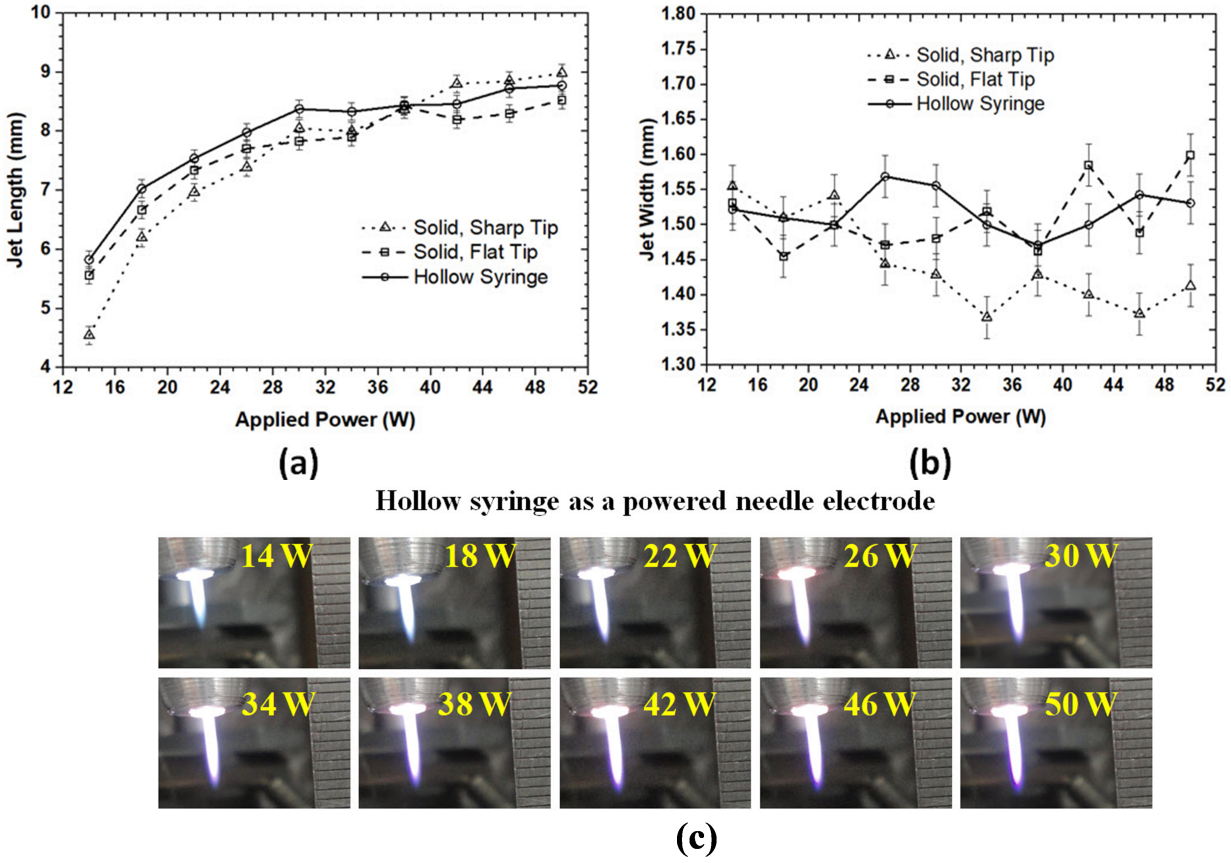

Figure 6. The length (a) and waist thickness (b) of the output jets versus different geometries of needle electrodes (solid with flat tip, solid with sharped tip, hollow syringe) with different applied powers; The length and diameter of the needle, the gas flow rate (argon) and outlet nozzle diameter, respectively, were 19 mm (corresponding to a discharge gap of 5 mm), 1.2 mm, 3 slm and (c) Images of plasma microjets, as examples, produced by different applied powers for hollow syringe electrode.

output power of 300 W and frequency of 13.56 MHz as shown schematically in Fig. 3. The reported powers in figures are the input powers to the plasma jet system shown in the RF power source display. The measurements were carried in our laboratory (higher than sea level) where a relative humidity of 40% and a room temperature of 27°C are typical.

The electrical properties of the discharge were studied by measuring the voltage applied on the powered electrode and discharge current. The discharge currents are obtained by measuring the potential deference across a 3.3 nF Capacitor placed in the grounded branch of the circuit. The data are registered by a four channels 300 MHz bandwidth digital oscilloscope (GW Instek GDS2304A) with a sampling rate of 2 GS/s and averaging over 256 samples, through a high voltage probe (Pintek HVP-39Pro).

In Fig. 4, a typical current and voltage waveforms are shown which have been recorded at 30 watts applied power. The total current, measured from the grounded electrode branch of the circuit, is composed of both the displacement and conductive currents.

$$\mathbf{J} = \mathbf{j} + \frac{1}{4\pi}\frac{\partial \mathbf{D}}{\partial t} = \mathbf{j} + \frac{\partial \mathbf{P}}{\partial t} + \frac{1}{4\pi}\frac{\partial \mathbf{E}}{\partial t} \qquad (1)$$

where $(1/4\pi)\partial\mathbf{D}/\partial t = \partial\mathbf{P}/\partial t + (1/4\pi)\partial\mathbf{E}/\partial t$ and $\mathbf{j}$, respectively, are the displacement and convective currents. The term $\partial\mathbf{P}/\partial t$ in the displacement current is connected with the motion of charges and indeed a current density but the term $(1/4\pi)\partial\mathbf{E}/\partial t$ is not related to charge motion and therefore, is not literally a current. To eliminate the term $(1/4\pi)\partial\mathbf{E}/\partial t$ from the experimentally measured current we have registered the current signal in plasma off state too. As is shown in Fig. 4a, the current measured in plasma off state is sinusoidal, however, the total current have oscillatory structure with a sinusoidal trend. All of the three plasma on, off, and discharge total charge current (obtained by subtraction of the plasma off current from the plasma on one) are shown in Fig. 4b.

The highest peak of the current signal, located on the rising section of the applied voltage in the plasma on state, is the main peak and illustrating the current of the discharge resulting from the applied RF power. The other few additional peaks which can be seen in the discharge current diagram, indicate additional micro discharges happening inside the system. These could be attributed to the multi-discharge regime, when a high power is applied to the system. But in our case where the power is not very high, these peaks may

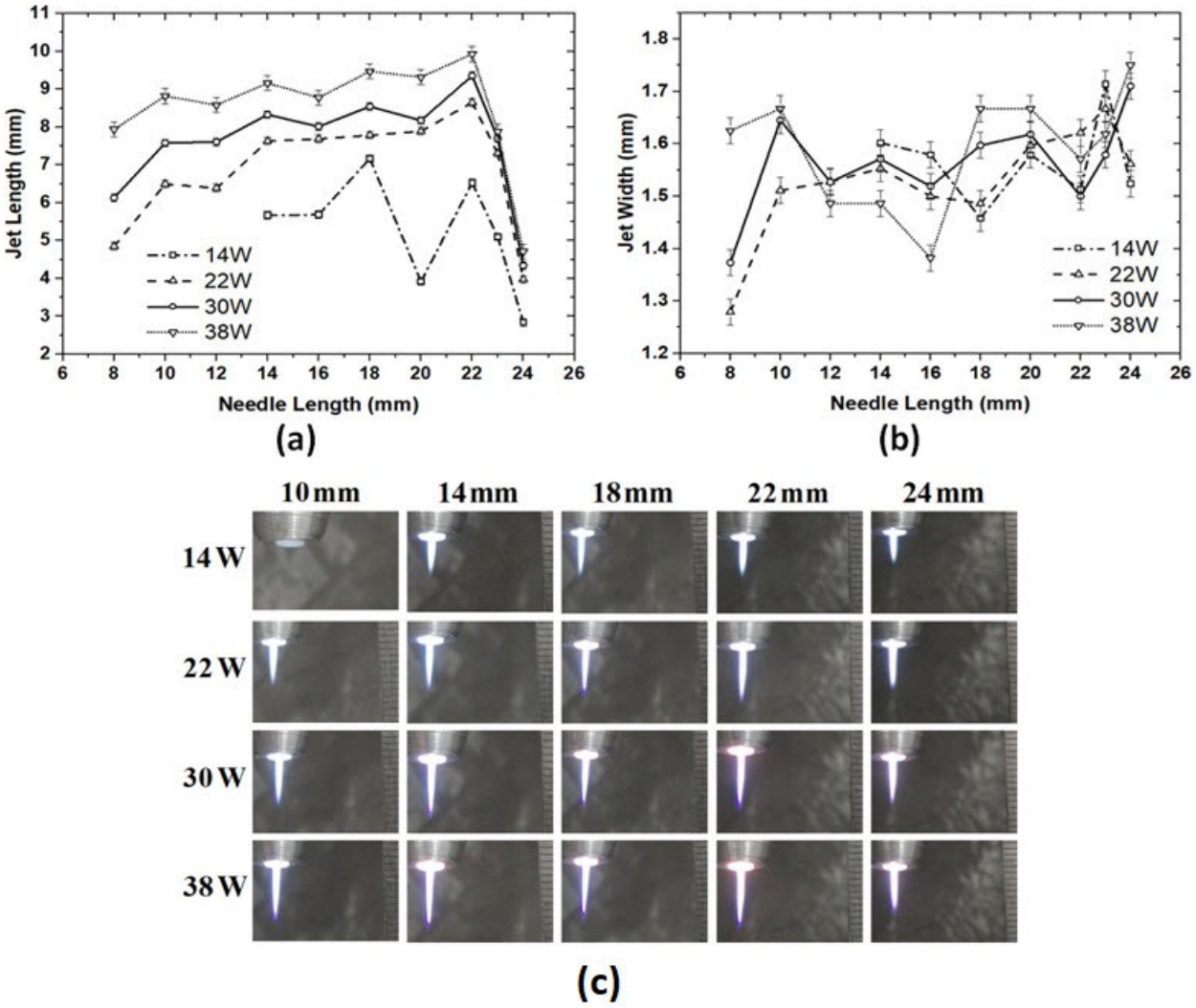

Figure 7. Length (a) and widths (b) of the output jet versus different needle length (corresponding to the gap sizes of $0.2 - 16$ mm). (c) Images of plasma microjets produced with different applied powers and discharge gaps with a constant gas flow rate of 3 slm.

attributed to micro discharges between needle/grounded electrodes and the dielectric, resulting from charges accumulated on the dielectrics.

In the plasma off state, the phase difference between the current and the voltage is nearly. The measured capacitance of our prototype system in this plasma off state (using the RLC meter of KDK Kokuyo Electric Co. Ltd: KC-605) is 1.8 pF which corresponds to a capacitive impedance of ≈ 40 kΩ. With the ignition of the plasma the current signal deforms and increases. The total current in this plasma on state has a large amplitude pulse at the up-rise of the voltage signal which can be an indication of bullet formation [27]. The voltage also decreases compared to that for the plasma off state. The phase difference between the voltage and the current reduces significantly in this case indicating that the plasma ignition introduces a parallel nonlinear load into the electrical circuit decreasing the capacitive impedance of the circuit. This effect is shown in Fig. 5 where the slope of the $V - I$ curve for the plasma on state is lower than that for the plasma off state.

3.1 A. The effects of powered electrode type

Different types of inner electrode such as hollow syringes, solid with flat tip, and solid with sharped tip are located into the device and the lengths and widths of the visible portions of the generated argon plasma microjets are measured at different RF input powers. The results are shown in Fig. 6. The measurements of the plume lengths and widths are carried out using the images taken by a digital camera (Sony DSC-W350) as illustrated schematically in Fig. 3. Measurements were made on two consecutive days and no significant difference was observed between the measured length and width of the visible column, except for small fluctuations. For each measurement item (each point in the graphs), the average of these measurements is taken into account, and the uncertainty in detecting the length and width of the jet from the pixels of the image is taken into consideration, then the error bars are calculated and determined.

It can be seen from Fig. 6a that the length of the jet increases with the power increment for all of the three types

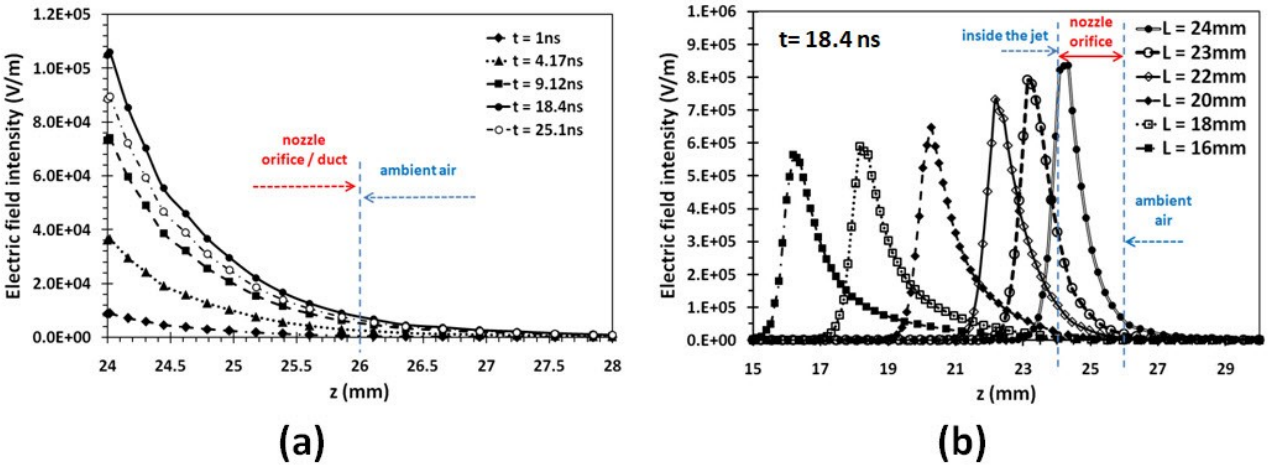

Figure 8. The electric field intensity (a) along the jet axis near the nozzle duct zone ($24-26$ mm) at different times, (b) at 18.4 nF in every period for different needle length.

of needle electrodes in the same trend leading to saturation at nearly input power of 30 W, but the stainless steel hollow powered electrode generates the longest plasma jet up to 38 W. This kind of behaviour is the same as for kHz plasma jets which has been reported before by Zhu et al. [28]. It is interesting to note that there is a convergence power point, 38 W, in which the length and width of jets are the same for these three electrode types and after this point, the hollow needle jet length/width fall behind the sharp-tip/flat-tip solid needle one, respectively. It is obvious from Fig. 6b that the widths of the jets from solid sharp-tip powered electrode decreases slightly with increasing power while remains nearly constant for the solid flat-tip one. The width of jets from hollow syringe show alternate structure with the first local maximum at about 26 W.

Although, the applied power directly affects the length of the output jet, but the amount of applied power to the system has its own technical and operational limitations. If the power is too high, or the flow rate is too low, arcing occurs at the end of the central electrode which streams in upstream direction. It has to be mentioned that input powers of higher than 40 watts seriously damage the powered electrode and the dielectric between the electrodes. Therefore the majority of our experiments carried out below 40 W.

Considering the above results, the hollow syringe needle electrode can be chosen as the best of the three electrode types, in this power range, so the remaining experiments were done using with this needle electrode type.

3.2 B. The effects of discharge gap size

The inter-electrode space (discharge gap) is an important parameter for expressing the intensity and profile of the electric field in the discharge space. Syringes with different length (8, 10, 12,..., 23.8 mm) corresponding to discharge gap sizes of 16, 14, 12,..., 0.2 mm respectively, are placed in the device and the output jet lengths and widths are measured for various input powers (Fig. 7). It is worthwhile to mention that the total depth of the device (24 mm), avoiding the nozzle blockage was limiting the maximum length of the needle electrode to 23.8 mm.

Fig. 7 shows that discharge gap of 2 mm (needle length of 22 mm) results in the longest jet. It has been explained by Yue and co-workers [25] that the propagation of the plasma bullet is determined by the electric field strength so that with a strong electric field the electron temperature is high, consequently, the intensity of the light emission is high, and the discharge propagates fast. They have also found that the polarity of the plasma plume is initially decided by the direction of the radial component of the applied electric field. Therefore in a positive discharge, the radial component of the electric field drives the electron drift from the surrounding area to the centre of the plume raising the electron density in the dark channel behind it. In this way, by reducing the voltage drop in the dark channel, a high voltage is applied to the plasma bullet and causes it to propagate faster and to farther distant. It would be reasonable to say that at the inter-electrode distance of 2 mm the electric field finds an optimum value with a large radial component toward the plume center and accelerates the ions outward leading to an increase in the length of the plasma plume.

We have simulated the axial and radial components of the electric field, at the output nozzle of the device, using AC/DC module of COMSOL multi-physics software applying time varying radiofrequency voltage to the needle electrode. Fig. 8a shows the electric field intensity in the nozzle duct at different times. It is obvious that at the times higher than 18.4 ns, corresponding to the peak of the applied voltage (a quarter of the RF period), for example, in $t = 25.1$ ns, the field strength in the given position is decreasing.

The intensity of the electric field at $t = 18.4$ ns (at the positive peak of the applied RF power), along the jet axis near the nozzle zone for different values of the needle lengths is shown in Fig. 8b. We note that the position of the peaks from the vertical dashed line (blue) in this figure shows the discharge gap for the corresponding needle electrode. It can be seen that the electric field at this position becomes more intense with increasing needle length (decreasing inter-electrode distance). The electric field intensity versus radial distance from the plasma jet axis is also shown in Fig. 9. It is evident that the electric field is concentrated near the axis

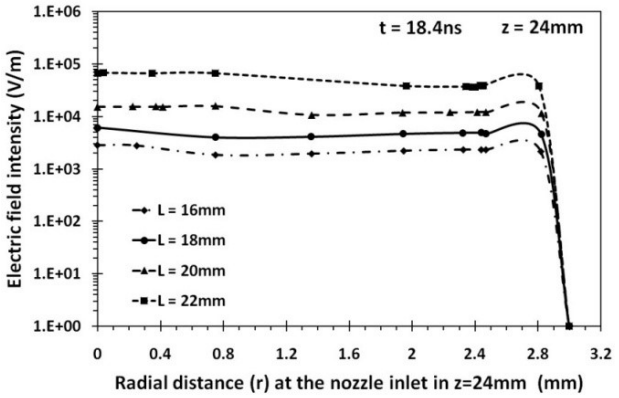

Figure 9. The electric field intensity in the nozzle inlet at different radial positions.

and decreases rapidly at the off-axis positions.

The output of the COMSOL simulation for electric field lines at different locations is shown in Fig. 10. Although considering the effects of electric discharge may strongly affect the field distribution, it is understood that the charged particles produced by the plasma are accelerated out of the nozzle in the same direction as the electrostatic field illustrates. Furthermore, in the presence of the ionization front (propagating along the jet axis, which is not simulated in this study), the electric field is disturbed, at the front of the ionization wave, the electric field becomes much stronger than elsewhere, which it will cause further acceleration of charged particles.

Briels and coworkers [29] with reference to their experimental confirmation [30, 31] have pointed out that the streamer inception and initial propagation is determined by the applied voltage and the electrode geometry. They have argued that, although the electric field, localized at the head of ionization wave, is sharply intense and disrupts the background electric field, however, the positive argon ions along with the ionization wave are driven by the electric field of the needle tip.

Referring to Fig. 8b, and bearing in mind the discussions presented by Yue [25] and Briels [29] as well as the obstruction effects and also divergence of the field lines due to the proximity of the two powered and grounded electrodes for needle lengths greater than 22 mm, the longer jet output would be justified for a gap distance of 2 mm.

3.3 C. Flute-like powered electrode

In all of the above experiments, the working gas and plasma enters into the hollow powered inner electrodes from their tip. A question arises in the mind that if we allow gas and plasma to enter from the side surface of the needle electrode at different positions, what effect will it have on the characteristics of the produced jet? To investigate this, we have made twin orifices (two holes located at the opposite ends of syringe diameter) around the syringes at different positions, measured from their tips. Choosing syringes with same diameters and fixing the gas flow rate at 3 slm, the variation of the jet lengths and widths versus the positions of the twin orifices for different input powers are measured and shown in Fig. 11. The trends of the variation of the jet length with the input power is nearly the same as for the previous case shown in Fig. 6a while in most cases the jets are shorter and wider than the corresponding ones for the simple hollow syringe. The jet lengths versus the orifice positions indicate local maxima at 6 may be 10 mm, 16 and 22 and minima at 8, 14 and 20 mm. The averaged value for errors on the orifices positions have been evaluated to be 1 mm. To show the reproducibility we have repeated the experiments, using the same needle electrodes, several timed and found that the maxima and minima appear in the same positions.

There is a similarity between the perforated powered electrode and the open acoustic tubes (flute like instruments) therefore it is reasonable to expect that the position of the maxima in the jet length follows the formulation of open acoustic tubes. It is well known that atmospheric pressure plasmas readily support acoustic pressure waves (50 Hz to 20 kHz) [32] and ultrasound pressure waves ($20-600$ kHz) [33, 34]. In these plasmas the role of ions is the same as neutral atoms in normal sound energy. However, in the case of the ions, they gain energy from the electromagnetic field that is produced by the repetitive power source. The difference between neutrals and ions is that ions (and electrons) absorb electrical energy from the electrical field with the plasma expansion and loses electrical energy with the plasma contraction in the off period of the repetitive drive frequency. These oscillations along with the motions of neutrals, cause fluctuations in speed of particles. The fluctuation in the speed of neutrals and ions therefore generate both sounds waves and an oscillatory electric field. With this perspective, the existence of these local maxima may be correlated with the ion-acoustic wave resonances inside the hollow needle electrodes that are in the kHz to MHz frequency ranges [35, 36] or correlated with the electron waves, which requires more experiments with higher accuracy and

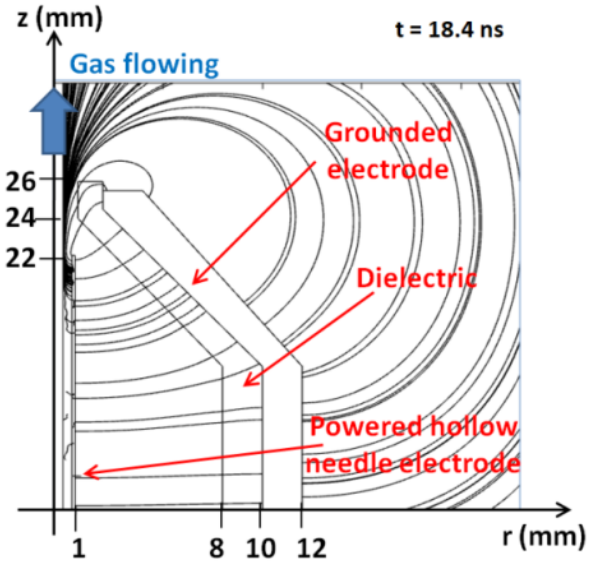

Figure 10. The distributions of the electric field lines at the nozzle duct. The voltage amplitude of 1 kV is used in this simulation by 13.56 MHz RF wave.

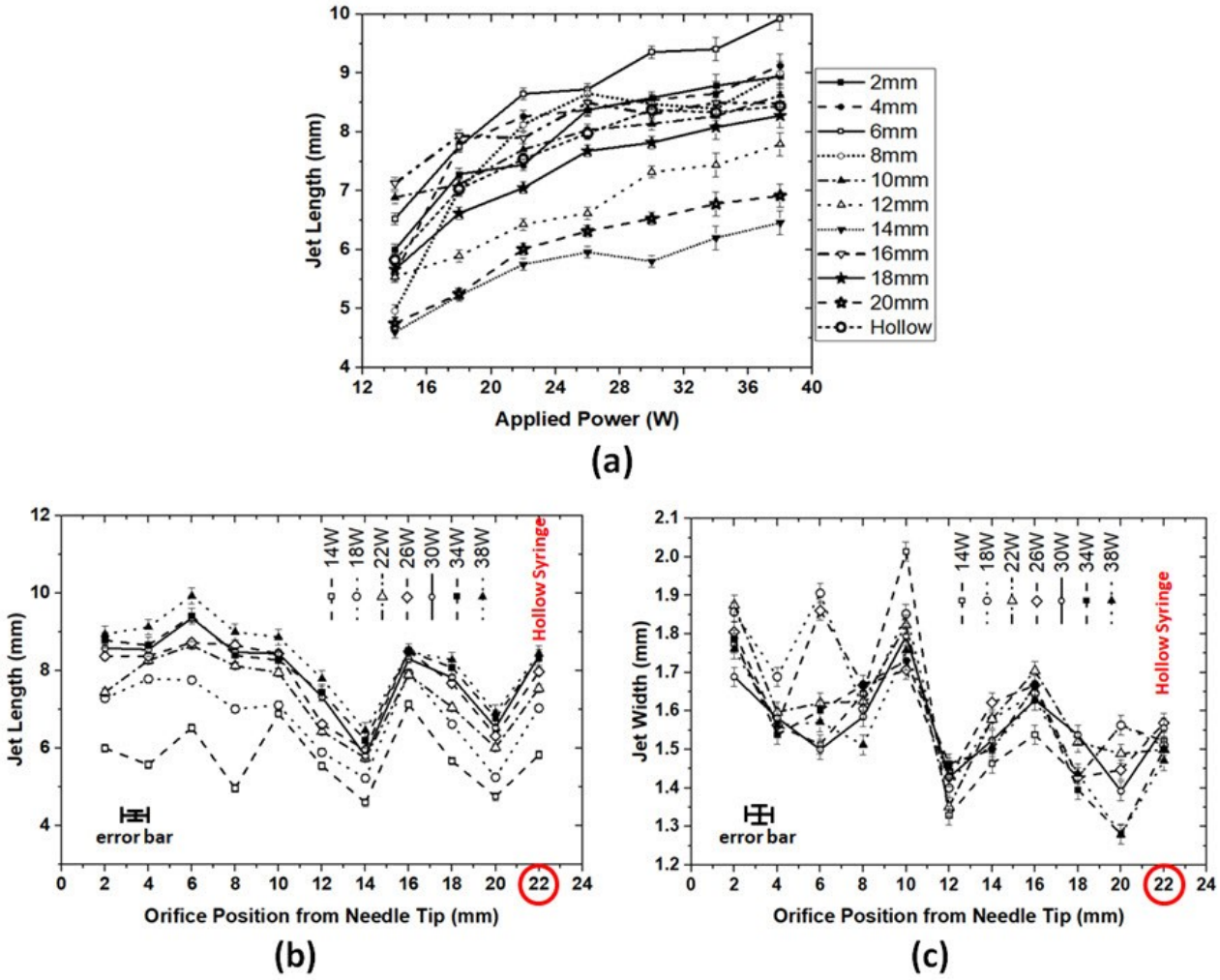

Figure 11. Outlet jet length for different positions of the perforation in the needle body. The gap between the needle and dielectric is measured from the needle tip.

remains as a question for future works.

3.4 D. Hollow powered electrode with different depth

In the previous sections we noted that the hollow syringe powered electrode showed better output and also the flute type electrodes indicated local maxima in the jet length versus input power with as suspicious association with ion-acoustic amplification. Due to the similarity of perforated needles with open acoustic tubes, it remains to be seen whether this similarity exists in hollow needles with different depths (i.e. closed acoustic tubes). To find out if there are any similarities between hollow needles and closed acoustic tubes, we have made several hollow syringe electrodes with different depth by collapsing syringes at different positions, measured from their tips, and located into the device. The lengths and widths of ejected argon jets at different RF powers are measured and plotted in Fig. 12. The variation of the jet lengths versus input power is the same as the results shown in Fig. 6a and Fig. 11a, indicating a saturation at a given point. Comparing Fig. 11 and Fig. 12 one can see that the jets are considerably narrower and slightly longer in the second one. There are, again, local maxima at 4, 10 mm and maybe at 14 or 16 mm hollow electrode depth and local minima at 2, 8 mm and maybe at 12 mm (Fig. 12b).

It should be mentioned that a needle-nose plier was used to block the needle electrode end by compressing the needle at the desired location leading to an averaged error of 1.2 mm in the hollow depth of the needle electrodes. Further research in this context is again left open.

4. The effects of the fluid factors on the produced jet

4.1 A. Diameter of nozzle outlet

The outlet nozzle hole determines the microjet width and has a significant role in its formation. Choosing a hollow needle electrode with inner diameter of 0.9 mm and thickness of 0.15 mm and adjusting the discharge gap to be 2 mm the effects of the diametric size of Teflon output nozzle on dimensions of the launched plasma microjet, with a gas flow rate of 3 slm is studied. Four similar nozzles with orifice diameters of 0.5, 1, 1.5 and 2 are used in different experiments at various applied RF powers. In the case of the 0.5 mm nozzle diameter, the plasma was formed around the needle inside the system but the plasma jet either

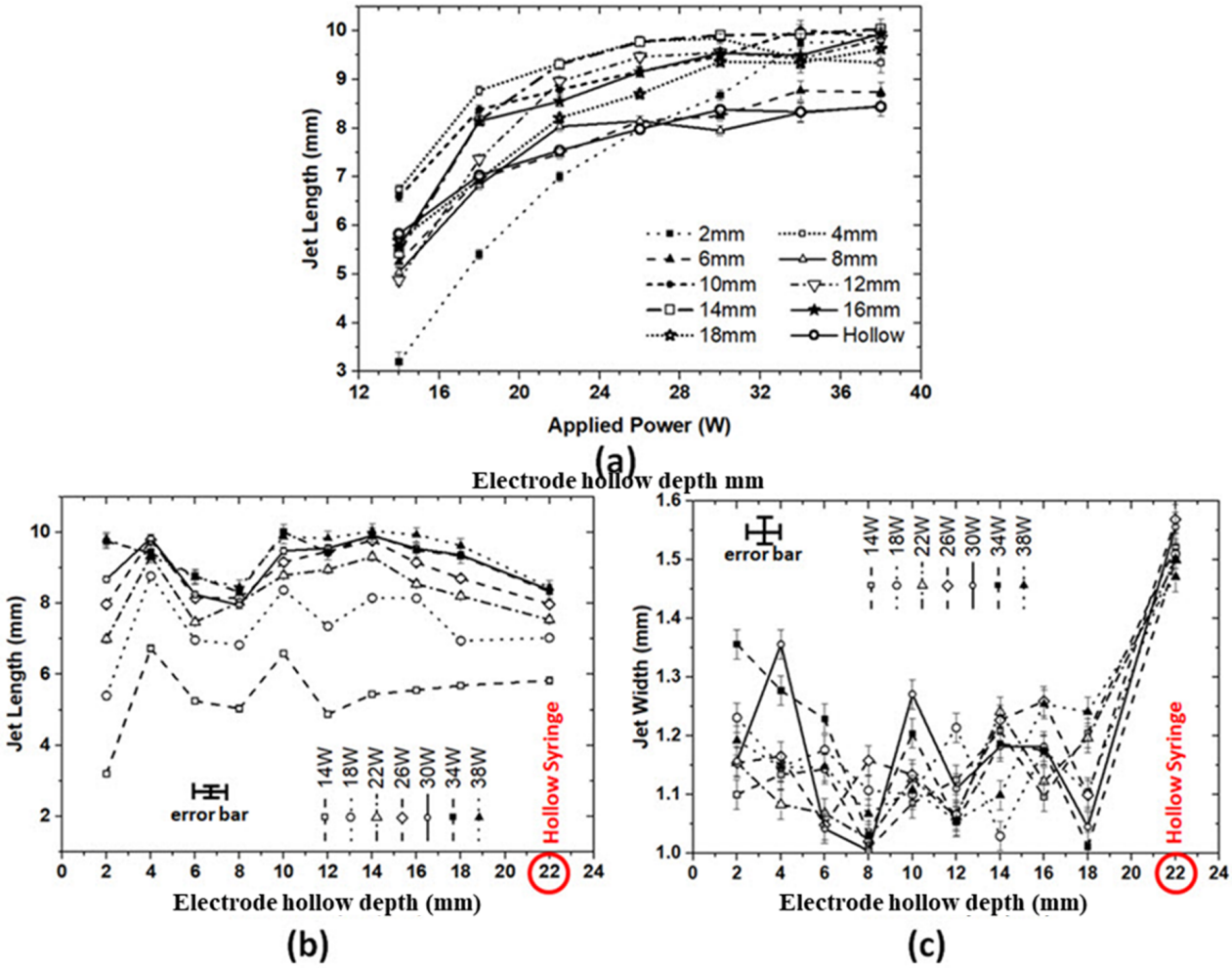

Figure 12. Variations of the plasma jet lengths and widths versus the RF input power with syringe powered inner electrode collapsed at different positions measured from their tips. The hollow depth of 22 mm corresponds to the total depth of syringe, which is marked with red colour.

was not formed or did not spread through the nozzle. The narrowest microjet is produced using the 1 mm nozzle but with not very long jet length (see Fig. 13). It can be seen, from this figure, that the optimal nozzle diameter is 1.5 mm, generating the longest microjet with relatively low thickness. With 2 mm hole diameter, the length-to-width ratio of the generated microjet is less than for the 1.5 mm orifice diameter.

In 2015, Ji et al. [37] observed that the length of the plasma plume generated inside hollow-core-fibre, using helium as the working gas, increases with the decreasing diameter of the fibre hole. They believed that the decreased tube diameter results in the increased gas flow velocity and the long-life species driven by the gas flow may move further to the downstream area, facilitating the increase of the plume length. Therefore, our result, showing an optimum 1.5 mm inner diameter for output nozzle with argon as the feed gas, is different from their result. Ji et al. explained that the long-life species, maybe the helium meta-stable excited atoms or ions, can be responsible for their results. Therefore, it can be deduced that argon metastable atoms or ions are not generated sufficiently in our experiments.

Another possible affecting factor is the Reynolds number and/or gas pressure inside the tube which is dependent on the outlet nozzle diameter. Viscous flow can generally be divided into laminar flow occurring at low flow rates and turbulent with corresponding vortex motion modes [38, 39]. Calculation of the Reynolds number and the flow value where laminar flow occurs depends on the geometry of the flow system as well as on the flow pattern. The common example is flow through a pipe, where the Reynolds number is defined as:

$$\mathrm{Re} = \frac{uD_H}{v} \tag{2}$$

where u, D_H and v are, respectively, the mean speed of the fluid in (m/s), hydraulic diameter of the pipe in (m), and kinematic viscosity of the fluid in (m^2/s). The latter is dependent on the pressure and temperature and for argon at 45°C is $\sim 14.82 \times 10^{-6}$ m^2/s. Jin and Wu and their co-workers [40,41] reported that the length of the He, Ne, or Ar plasma plume inside a glass tube increases with an increase in the gas flow rate under laminar flow, characterized by the Reynolds numbers up to 2300, while it decreases as the Reynolds number further increases in the laminar-to-

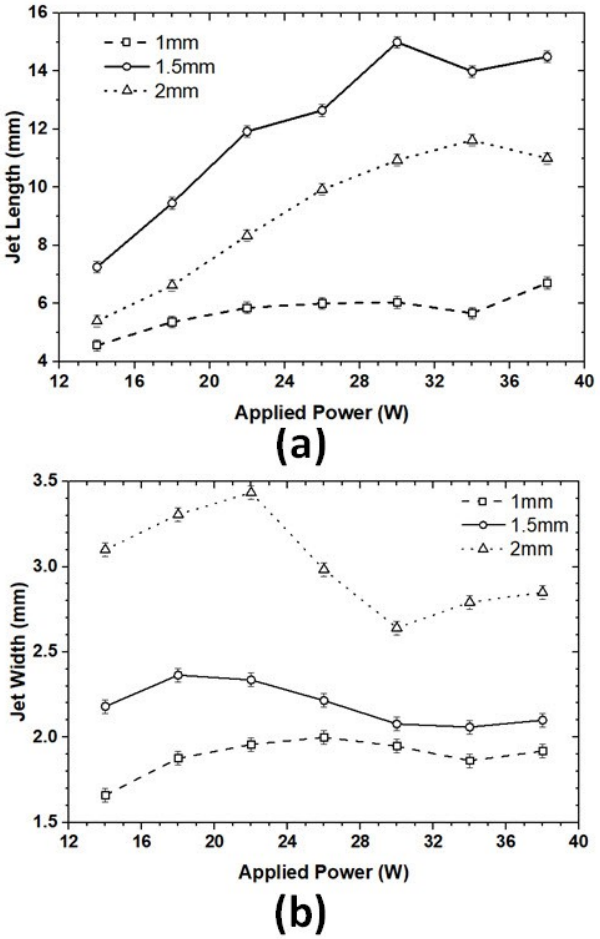

Figure 13. Length (a) and thickness (b) of output jet versus the orifice diameters. The Reynolds numbers for the nozzle hole diameters 1, 1.5 and 2 mm are, respectively, 4296, 2864 and 2148.

turbulent transition region. The Reynolds number decreases with increasing the tube diameter. Therefore, according to these research works, the plume length should be constant, with the tube diameter increment, while in our work the plume length has an optimum point of 1.5 mm tube diameter.

Increasing the nozzle diameter to values higher than the optimum value led to shortening, as well as broadening of the plasma jet in our experiments. It may seem that by increasing the gas flow rate at this stage, it would be possible to increase the jet length but the data from our experimental results show that the feed gas flow has an optimum value (see next section). Therefore, we have found that the diameter of 1.5 mm for the output nozzle, together with the gas flow rate of 3 slm corresponding to a Reynolds number of 2864, yields a longer microjet. This result is in good agreement with the Wu's result [41] obtained at the Reynolds number of 2386, corresponding to a nozzle diameter of in our case (we do not have data in this nozzle diameter).

4.2 B. Gas flow rate and output microjet dimensions

The effect of feed gas flow rate on the dimensions of the plasma jet is studied with two different RF input powers of 15 and 26 watts. As shown in Fig. 14a, the jet length reaches to local maxima at the flow rate of 2.5 slm for both input powers. The jet width increases linearly with gas flow rate (14b).

These are in agreement with previously reported results [40]. A similar trend was reported for the argon plasma jet operating at 13 kHz [42].The change in the plasma jet length as a function of gas flow rate has been observed previously with helium and air plasma jets [41,43].

It has to be mentioned that at higher flow rates, the plume becomes unstable and the previously conical form of the jet head becomes well rounded and then begins to decrease due to flow turbulence [44]. The gas flow rate higher than 2.5 slm up to 5.5 slm indicate the transition zone and the plume length begins to decrease. The Reynolds numbers are 1910, 2386, 2864, 3340,..., 5728 for different gas flow rates of 2, 2.5, 3, 3.5 and 6 slm, respectively. The longest microjet length corresponds to the Reynolds number of 2386 where the turbulent phase is enough low.

The Reynolds number can be related to the pipe diameter, d, and the gas flow rate, Q, as follows:

$$\mathrm{Re} = \frac{Q}{\pi D_H \nu} \tag{3}$$

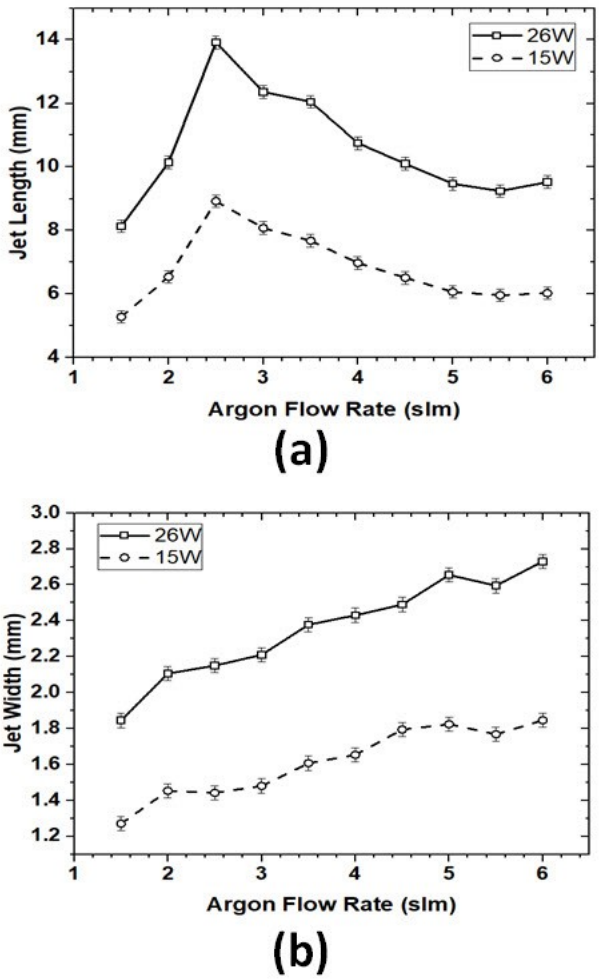

Figure 14. The lengths (a) and jet diameters (b) versus argon gas flow rates under applied RF powers of 15 and 26 watts.

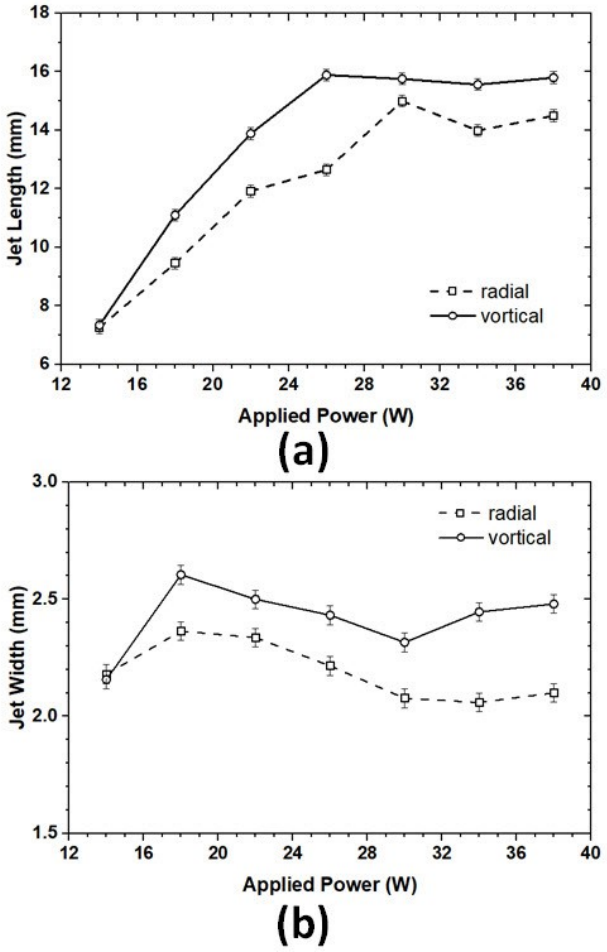

Figure 15. Length (a) and diameter (b) of the output jet in two different gas injection manner.

For optimal operation of the jet device, a suitable ratio between the size of the outlet hole, d, and the flow rate, Q, must be found to obtain a laminar flow and avoid turbulence.

When the plasma jet operates in the laminar mode, the ambient air flow into the plasma jet is small and depends slightly on its velocity. In this mode, increasing the flow rate reduces the concentrations of air in the argon column, leading to an increase in the length of the jet. Then, once the transition-to-turbulence occurs, the mixing of working gas with air reduces the length of the jet and transport mechanisms dominate in the turbulent mode [45].

4.3 C. The effects of gas injection method

The effects of feed gas entry into the system on the generated plasma microjet is investigated using two types of gas injection structures, radial and tangential (or vortical) shown Fig. 1b. The dimensions of the plume were measured at different input RF powers which are plotted in Fig. 15. The results indicate a significant increase in the plasma jet length and width in vortical injection method.

In vortical mode, the cyclonic rotational motion of the argon atoms may help the gas flowing laminar as layer-by-layer. The Reynolds number in vortical mode is lower.

5. Conclusion

An atmospheric pressure plasma microjet (APPμJ) device with a tapered ground electrode is developed. The size of the constructed prototype together with its on-built BNC connection is 38mm $\times$ 15mm, which can be made even smaller using sophisticated manners. The working gas entrance is designed so that the gas could be injected straight along the radial direction or with a vortex type motion with a possible maximum angular velocity. The system is designed such that the replacement of its parts to be very easy.

The effects of the powered electrode geometry and the amount of input power, on the launched RF plasma jets are investigated. Different types of inner powered-electrode such as hollow syringe, solid flat-tip, and solid sharp-tip are located into the device and the lengths and widths of the visible portions of the generated argon plasma microjets are measured at different RF input powers and the results are plotted and interpreted. It is found that the length of the jet increases, for all types of needle electrodes, with the power increment in the same trend leading to saturation at input power of about 30 W, with the longest plasma jet, up to the input power of 38 W belonging to the hollow electrode. This point (input power of 38 W) serves as a convergence point in which the length and width of jets are the same for all the three electrode types and after this point, the hollow needle jet length/width left behind the sharp-tip/flat-tip solid needle one, respectively. Inserting hollow syringes of different length inside the device and thus changing the discharge gap size, the longest plasma jet is obtained by 2 mm discharge gap. The axial and radial components of the electric field and the field intensities are simulated at the device output nozzle by applying radiofrequency voltage to the needle electrode and the above mentioned effects are rationalized.

To investigate the effect of the gas inlet from the side of syringes instead of from their tip into them, twin orifices at the opposite ends of syringe diameter at different axial positions are made. Choosing syringes with the same diameters and fixing the gas flow rate at a given amount, variation of the jet lengths and widths versus the positions of the twin orifices for different input powers, are measured. The trend of jet variation versus the input power is nearly the same as for the simple hollow syringes, but for the most cases the jets are shorter and wider than the corresponding ones. The jet lengths versus the orifice positions indicate, also, local maxima and minima at some positions which left as a future research question. They may be related to the resonant modes of the open acoustic tube.

To find out if there are any similarities between hollow needles and closed acoustic tubes, several hollow syringe electrodes with different hollow depths are made by collapsing syringes at different positions and located into the device, thus, keeping the discharge gap at a constant value of 2 mm. The lengths and widths of the plasma plumes versus input RF powers are measured. The same trend of the plume length and width variation with input power, indicating a saturation at a given point, is obtained but the overall jets length were longer compared to the

corresponding quantities from flute like need electrodes. The results also indicated, again, the local maxima and minima for plume length.
It has been explained that reducing the outlet nozzle diameter have to increase the microjet length via increasing the gas flow velocity as well as making the long-life species driven by the gas flow to farther downstream areas. However, an opposite result obtained in our case with argon feed gas, and the plume length showed a local maximum 1.5 mm inner diameter of nozzle output. This behaviour was related to low number density of long-life argon meta-stable species.
Investigating the effects of gas flow rates at two different input powers of 15 and 26 watts, the microjet length found a local maximum at 2.5 slm, regardless of input power values. In flow rates above 2.5 slm, the laminar-to-turbulent transition occurred, and the plume length began to decrease. The effects of how the working gas enters the system, on the generated plasma microjet, is investigated using two types of gas injection structures of radial and vortical. The results indicated a significant increase in the plasma jet length and width in vortical injection. This increase could be due to the strengthening of the laminar phase by cyclotron motion of argon in nozzle's outlet.

Conflict of interest statement:
The authors declare that they have no conflict of interest.

References

[1] U. Kogelschatz. "Dielectric-barrier discharges: their history, discharge physics, and industrial applications". *Chem. Plasma Processing*, **23**:1, 2003.

[2] H. E. Wagner, R. Brandenburg, K. V. Kozlov, A. Sonnenfeld, P. Michel, and J. F. Behnke. "The barrier discharge: basic properties and applications to surface treatment". *Vacuum*, **71**:417, 2003.

[3] R. Foest, M. Schmidt, and K. Becker. "Microplasmas, an emerging field of low-temperature plasma science and technolog". *Int. J. Mass Spectrom*, **248**:87, 2006.

[4] S. Rupf, A. Lehmann, M. Hannig, B.Schäfer, A. Schubert, U. Feldmann, and A. Schindler. "Killing of adherent oral microbes by a non-thermal atmospheric plasma jet". *Journal of Medical Microbiology*, **59**:206, 2010.

[5] R. E. J. Sladek, E. Stoffels, R. Walraven, P. J. A. Tielbeek, and R. A. Koolhoven. "Plasma treatment of dental cavities: a feasibility study". *IEEE Trans. Plasma Sci.*, **32**:1540, 2004.

[6] J. Y. Jeong, S. E. Babayan, V. J. Tu, J. Park, R. F. Hicks I. Henins, and G. S. Selwyn. "Etching materials with an atmospheric-pressure plasma jet". *Plasma Sources Sci. Technol.*, **7**:282, 1998.

[7] H. Koinuma, H. Ohkubo, T. Hashimoto, K. Inomata, T. Shiraishi, A. Miyanaga, and S. Hayashi. "Development and application of a microbeam plasma generator". *App. Phys. Lett.*, **60**:816, 1992.

[8] E. Stoffels, A. J. Flikweert, W. W. Stoffels, and G. M. W. Kroesen. "Plasma needle: a non-destructive atmospheric plasma source for fine surface treatment of (bio) materials". *Plasma Sources Sci. Technol.*, **11**:383, 2002.

[9] R. Stonies, S. Schermer, E. Voges, and Jose A. C. Broekaert. "A new small microwave plasma torch". *Plasma Sources Sci. Technol.*, **13**:604, 2004.

[10] M. Teschke, J. Kedzierski, E. G. Finantu-Dinu, D. Korzec, and J. Engemann. "High-speed photographs of a dielectric barrier atmospheric pressure plasma jet". *IEEE Trans. Plasma Sci.*, **33**:310, 2005.

[11] M. Laroussi and X. Lu. "Room-temperature atmospheric pressure plasma plume for biomedical applications". *Appl. Phys. Lett.*, **87**:113902, 2005.

[12] Y. C. Hong and H. S. Uhm. "Microplasma jet at atmospheric pressure". *Appl. Phys. Lett.*, **89**:221504, 2006.

[13] E. P. van der Laan, E. Stoffels, and M. Steinbuch. "Development of a smart positioning sensor for the plasma needle". *Plasma Sources Sci. Technol.*, **15**:582, 2006.

[14] G. van de Ven. "Design of a guiding mechanism for the plasma needle". *Technische Universiteit Eindhoven*, **2006.049**, 2006.

[15] D. B. Kim, J. K. Rhee, S. Y. Moon, and W. Choe. "Study of geometrical and operational parameters controlling the low frequency microjet atmospheric pressure plasma characteristics". *Appl. Phys. Lett.*, **89**:061502, 2006.

[16] J. F. Kolb, A. A. H. Mohamed, R. O. Price, R. J. Swanson, A. Bowman, R. L. Chiavarini, and K. H. Schoenbach. "Cold atmospheric pressure air plasma jet for medical applications". *Appl. Phys. Lett.*, **92**:241501, 2008.

[17] W. D. Zhu and J. L. Lopez. "A DC non-thermal atmospheric-pressure plasma microjet". *Plasma Sources Sci. Technol.*, **21**:034018, 2012.

[18] P. Sun, J. Pan, Y. Tian, N. Bai, H. Wu, L. Wang, C. Yu, J. Zhang, W. Zhu, K. H. Becker, and J. Fang. "Tooth whitening with hydrogen peroxide assisted by a direct-current cold atmospheric-pressure air plasma microjet". *IEEE Trans. Plasma Sci.*, **38**:1892, 2010.

[19] G. Wang, G. Ye, X. Yang, H. Pan, K. Sun, J. Zhang, J. Pan, and J. Fang. "The efficacy, safety, stability, and mechanism of tooth whitening by a cold atmospheric pressure air plasma microjet assisted with or without Hydrogen Peroxide". *IEEE Trans. Plasma Sci.*, **42**:1623, 2014.

[20] J. Pan, P. Sun, Y. Tian, H. Zhou, H. Wu, N. Bai, F. Liu, W. Zhu, J. Zhang, K. H. Becker, and J. Fang.

[21] R. Wang, H. Zhou, P. Sun, H. Wu, J. Pan, W. Zhu, J. Zhang, and J. Fang. "The effect of an atmospheric pressure, DC nonthermal plasma microjet on tooth root canal, dentinal tubules infection and reinfection prevention". *Plas. Med.*, **1**:143, 2011.

[22] R. Bussiahn, R. Brandenburg, T. Gerling, E. Kindel, H. Lange, N. Lembkea, K-D. Weltmann, Th. von Woedtk, and T. Kocher. "The hairline plasma: an intermittent negative dc-corona discharge at atmospheric pressure for plasma medical application". *Appl Phys Lett.*, **96**:143701, 2010.

[23] S. Tajima, S. Tsuchiya, M. Matsumori, S. Nakatsuka, and T. Ichiki. "Reduction of copper oxide films by an atmospheric-pressure inductively coupled plasma microjet". *Trans. Mater. Res. Soc. Japan*, **35**:621, 2010.

[24] D. Liu, Z. Zhang, Z. Liu, B. Wang, Q. Li, X. Wang, and M.G. Kong. "Plasma jets with needle–ring electrodes: the insulated sealing of the needle and its effect on the plasma characteristics". *IEEE Trans. Plasma Sci.*, **46**:2942, 2018.

[25] Y. Yue, F. Ma, W. Gong, J. Li, F. Yu, L. Nie, Y. Xian, K. Bazaka, X. Lu, and K. Ostrikov. "Radial constraints and the polarity mechanism of plasma plume". *Phys Plasmas*, **25**:103510, 2018.

[26] X. Lu, M. Laroussi, and V. Puech. "On atmospheric-pressure non-equilibrium plasma jets and plasma bullets". *Plasma Sources Sci. Technol.*, **21**:034005, 2012.

[27] X. Lu and M. Laroussi. "Dynamics of an atmospheric pressure plasma plume generated by submicrosecond voltage pulses". *J. Appl. Phys.*, **100**:063302, 2006.

[28] W-C. Zhu, Q. Li, and X-M. Pu. "Characteristics of atmospheric pressure plasma jets emerging into ambient air and helium". *J. Phys. D: Appl. Phys.*, **42**:202002, 2009.

[29] T. M. P. Briels, J. Kos, G. J. J. Winands, E. M. van Veldhuizen, and U. Ebert. "Positive and negative streamers in ambient air: measuring diameter, velocity and dissipated energy". *J. Phys. D: Appl. Phys.*, **41**:234004, 2008.

[30] T. M. P. Briels, E. M. van Veldhuizen, and U. Ebert.

[31] T. M. P. Briels, J. Kos, E. M. van Veldhuizen, and U. Ebert. "Circuit dependence of the diameter of pulsed positive streamers in air". *J. Phys. D: Appl. Phys.*, **39**:5201, 2006.

[32] M. Fitaire and T. D. Mantei. "Some experimental results on acoustic wave propagation in a plasma". *Phys. of Fluids*, **15**:464, 1972.

[33] T. Nakane. "Discharge phenomenon in a high-intensity acoustic standing wave field". *IEEE Trans. Plasma Sci.*, **33**:356, 2005.

[34] V. S. Soukhominov, V. Y. Kolosov, V. A. Sheverev, and M. V. ÖtÜgen. "Acoustic dispersion in glow discharge plasma: A phenomenological analysis". *Phys. of Fluids*, **14**:427, 2002.

[35] Z. Zhang, K. Xie, J. Ouyang, N. Guo, Y. Qin, Q. Xia, S. Bai, X. Wu, and Z. Gu. "Steady and oscillatory plasma properties in the near-field plume of a hollow cathode". *Plasma Sci. Technol.*, **20**:024010, 2018.

[36] Y. Qin, K. Xie, N. Guo, Z. Zhang, C. Zhang, Z. Gu, Y. Zhang, Z. Jiang, and J. Ouyang. "The analysis of high amplitude of potential oscillations near the hollow cathode of ion thruster". *Acta Astronautica*, **134**:265, 2017.

[37] L. Ji, Z. Bi, J. Niu, X. Zhang, R. Zhou, Y. Song, J. Liu, and D. Liu. "Effect of helium pressure and flow rate on microplasma propagation along hollow-core fibers". *J. Vac. Sci. Technol. A*, **33**:021302, 2015.

[38] G. Falkovich. *Fluid Mechanics*. Cambridge University Press, 2011.

[39] E. Stoffels, Y. A. Gonzalvo, T. D. Whitmore, D. L. Seymour, and J.A. Rees. "A plasma needle generates nitric oxide". *Plasma Sources Sci. Technol.*, **15**:501, 2006.

[40] D. J. Jin, H. S. Uhm, and G. Cho. "Influence of the gas-flow Reynolds number on a plasma column in a glass tub". *Phys. Plasmas*, **20**:083513, 2013.

[41] S. Wu, X. Lu, Y. Yue, X. Dong, and X. Pei. "Effects of the tube diameter on the propagation of helium plasma plume via electric field measurement". *Phys. Plasmas*, **23**:103506, 2016.

[42] Y. S. Seo, H. Wk. Lee, H. C. Kwon, J. Choi, S. M. Lee, K. C. Woo, K. T. Kim, and J. K. Lee. "A study on characterization of atmospheric pressure plasma jets according to the driving frequency for biomedical applications". *Thin Solid Films*, **519**:7071, 2011.

[43] R. Wang, W. Zhu, J. L. Re, J. Zhang, J. Fang, and J. L. Lopez. "Laminar-to-turbulent transition of a DC helium/oxygen (2%) plasma microjet". *IEEE Trans. Plasma Sci.*, **39**:2374, 2011.

[44] A. Konoa, T. Sugiyama, T. Goto, H. Furuhashi, and Y. Uchida. "Production of CW high-density non-equilibrium plasma in the atmosphere using microgap discharge excited by microwave". *Japanese J. Appl. Phys.*, **40**:238, 2001.

[45] K. Cheng, X. Chen, and W. Pan. "Comparison of laminar and turbulent thermal plasma jet characteristics—A modeling study ". *Plasma Chem. Plasma Process.*, **26**:211, 2006.